Interfacial particle bonding via an ultrathin polymer film on Al$_2$O$_3$ nanoparticles by plasma polymerization

Donglu Shi and Peng He
Department of Materials Science and Engineering, University of Cincinnati,
Cincinnati, Ohio 45221-0012

S.X. Wang
Department of Nuclear Engineering and Radiological Science, University of Michigan,
Ann Arbor, Michigan 48109

Wim J. van Ooij
Department of Materials Science and Engineering, University of Cincinnati,
Cincinnati, Ohio 45221-0012

L.M. Wang
Department of Nuclear Engineering and Radiological Science, University of Michigan,
Ann Arbor, Michigan 48109

Jiangang Zhao and Zhou Yu
Department of Materials Science and Engineering, University of Cincinnati,
Cincinnati, Ohio 45221-0012

To study interfacial particle-to-particle bonding mechanisms, an ultrathin film of pyrrole was deposited on alumina nanoparticles using a plasma polymerization treatment. High resolution transmission electron microscopy experiments showed that an extremely thin film of the pyrrole layer (2 nm) was uniformly deposited on the surfaces of the nanoparticles. In particular, the particles of all sizes (10–150 nm) exhibited equally uniform ultrathin films indicating well-dispersed nanoparticles in the fluidized bed during the plasma treatment. Time-of-flight secondary ion mass spectroscopy experiments confirmed the nano-surface deposition of the pyrrole films on the nanoparticles. The pyrrole-coated nanoparticles were consolidated at a temperature range (approximately 250 °C) much lower than the conventional sintering temperature. The density of consolidated bulk alumina has reached about 95% of the theoretical density of alumina with only a few percent of polymer in the matrix. After low-temperature consolidation, the micro-hardness test was performed on the bulk samples to study the strength that was related to particle-particle adhesion. The underlying adhesion mechanism for bonding of the nanoparticles is discussed.

I. INTRODUCTION

The current method of consolidating ceramics is through solid-state sintering at high temperatures above 1000 °C.[1–6] Sintered ceramic products represent a wide range of materials systems that may vary widely in the number of components, particle characteristics, complexity of chemical reactions, and densification mechanisms during sintering. The concept of sintering is based upon the joining of solid particles at interfaces through diffusion. However, such a process is thermally assisted requiring extremely high thermal energy especially for certain ceramics such as alumina. If these particles can be bonded strongly through other means such as an adhesive coating on the particle surfaces, it may serve as an alternative process to sintering. The low-temperature consolidation will reduce severe surface reactions, geometry distortion, and lower the processing cost because ceramic fabrication requires expensive furnaces and other atmosphere control facilities. Furthermore, in the recent development of electronic materials, ceramics are often composed with other types of materials including metals and polymers for device design and achieving unique physical properties. Such a composite cannot be easily processed at high temperatures together due to obvious reasons. It will only be possible to process these composites using a low-temperature consolidation method. The low-temperature consolidated ceramics will combine the advantages of both ceramic (rigid, hard, and abrasive) and polymer (can be processed at low temperatures).

As noted above, one of the possibilities in low-temperature consolidation is through an adhesive layer of polymer thin film between the ceramic particles. In this way, the polymer film acts as a nanoscaled adhesive (NSA) that bonds the ceramics particles together. Therefore the challenge in achieving such adhesive bonding lies primarily in the deposition of a polymer film on ceramic particles. Two important aspects in this approach must be noted: (i) this polymer film has to be extremely thin (a few nanometers thick), which makes it fundamentally different from the conventional synthesis where the binder material has a large volume fraction in the ceramic matrix. In this process, the resulting polymer is less than a few volume percent, and (ii) due to the adhesive nature of the polymer film, the ceramic particles may bond to each other; therefore, consolidate in a bulk form. It will be advantageous to have more contacting surfaces by using nanoparticles so that the consolidation is sufficiently strengthened by more adhesive interfaces in the ceramic matrix.

In this experiment we have attempted to coat a thin adhesive film of polymer onto alumina nanoparticles. After coating the experiments were focused on the consolidation of the coated nanoparticles at a temperature range much lower than the normal sintering temperature. High resolution transmission electron microscopy (HRTEM) was used to study the extremely thin film of the pyrrole layer (2 nm) on the surfaces of the alumina nanoparticles. Time-of-flight secondary ion mass spectroscopy (TOFSIMS) experiments were carried out to analyze the composition of the thin film on the nanoparticles. After low-temperature consolidation, a micro-hardness test was performed on the bulk samples to study the strength that was related to particle-particle adhesion. The underlying adhesion mechanism for bonding of the particles is discussed.

II. EXPERIMENTAL DETAILS

In this experiment, we selected nanoscale alumina particles ranging from a few nanometers to 150 nm. This large distribution of particles was particularly useful for the study of experimental deposition conditions for different sizes. The schematic diagram of the plasma reactor for thin film deposition of nanoparticles is shown in Fig. 1. The vacuum chamber of plasma reactor consisted of a Pyrex glass column about 80 cm in height and 6 cm in internal diameter.[7,8] The nanoparticles of alumina were vigorously stirred at the bottom of the tube and thus the surface of nanoparticles can be continuously renewed and exposed to the plasma for thin film deposition during the plasma polymerization process. A magnetic bar was used to stir the powders. The gases and monomers were introduced from the gas inlet during the plasma cleaning treatment or plasma polymerization. The system pressure
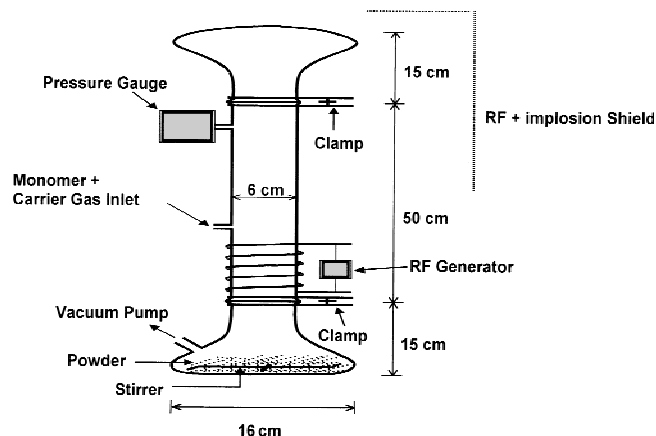

FIG. 1. Schematic diagram of the plasma reactor for thin polymer film coating of the nanoparticles.

was measured by a pressure gauge. A discharge by radio frequency (rf) power of 13.56 MHz was used for the plasma film deposition.

Before the plasma treatment, the basic pressure was pumped down to less than 2 Pa and then the plasma gases or monomer vapors were introduced into the reactor chamber. The operating pressure was adjusted by the gas/monomer mass flow rate. The base pressure was less than 1 Pa. Pyrrole was used as the monomer for plasma polymerization. During the plasma polymerization process, the input power was 10 W and the system pressure was 25 Pa. The plasma treatment time was 240 min/batch and 40 g of powder was treated.

After the plasma treatment, the nanoparticles of alumina were examined by using HRTEM, scanning electron microscopy (SEM), x-ray diffraction, and TOFSIMS. The HRTEM experiments were performed on a JEM 4000EX TEM. The TOFSIMS analyses were performed on an ION-TOF Model IV instrument. Vickers micro-hardness testing was used to determine the hardness values of consolidated bulk samples.

The consolidation of the coated nanoparticles was carried out in a straightforward fashion. After coating, both coated and uncoated powders were pressed into pellets with a 13-mm diameter die. The applied pressure for each pressing was 19 MPa. The pellets were then heat-treated in a box furnace in air. The heat treatment temperatures used were 250, 350, 550, and 800 °C. At each temperature the sample was held for various times: 60, 120, 240, 360, and 480 min. After heat treatment, the pellets were air cooled to room temperature.

III. RESULTS AND DISCUSSION

The original and nanocoated Al₂O₃ nanoparticles were dispersed onto the holy-carbon film supported by Cu-grids for transmission electron microscopy (TEM) operated at 400 kV. Figure 2(a) shows the HRTEM image of

the original, uncoated alumina nanoparticles. As can be seen in this figure, the particle size ranges between 10 and 150 nm. The particles exhibit a spherical shape for all sizes. Figure 2(b) is the high-resolution image of the original nanoparticles. The lattice image clearly shows the naked particle surface of alumina. Figure 3(a) is the bright field image of the coated nanoparticles. An ultra-thin thin film of pyrrole can be clearly seen over nano-particles of different sizes. The ultrathin film is marked by the double-lines in Figs. 3(a) and 3(b). The thickness of ultrathin film is approximately 2 nm and appears to be uniform surrounding the particle surface. Particularly im-portant, although these particles have different diameters, the film remains the same thickness indicating a uniform distribution of active radicals in the plasma chamber. Figure 3(b) is the high-resolution image of a particle with a uniform nanocoating. The ultrathin film is tightly

bound to the particles. The film was identified as typical amorphous structure by high-resolution electron micros-copy observation over different particles.

To confirm the TEM observations shown in Figs. 2–3, TOFSIMS was carried out to study the surface films of the nanoparticles. Figure 4(a) shows part of the nega-tive TOFSIMS spectrum of untreated nanoparticles of alumina. There were also traces of sulfur, iodine, and organic material. The positive spectrum (not shown here) also indicated some magnesium at the surface. In Fig. 4(b) one can see that the treated alumina has strong pyrrole cluster peaks indicating the surface coating of the nanoparticles and consistent with the HRTEM data presented in Figs. 2 and 3. The treated aluminum oxide shows the characteristic cluster pattern of plasma-polymerized pyrrole [Fig. 4(b)].[7] The intense peak at −26 m/z (CN$^-$) in Fig. 4(b) is typical of all
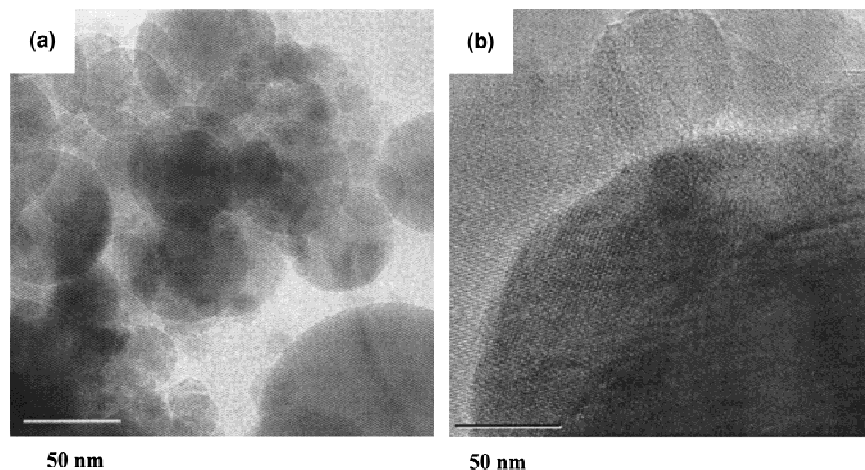

FIG. 2. (a) Bright field image of the original, uncoated alumina nanoparticles. A particle size distribution ranging from 10–150 nm can be seen in this figure (scale bar = 50 nm). (b) High resolution TEM images of the original particles showing crystal lattice and the uncoated nature of the nanoparticle surfaces (scale bar = 10 nm).
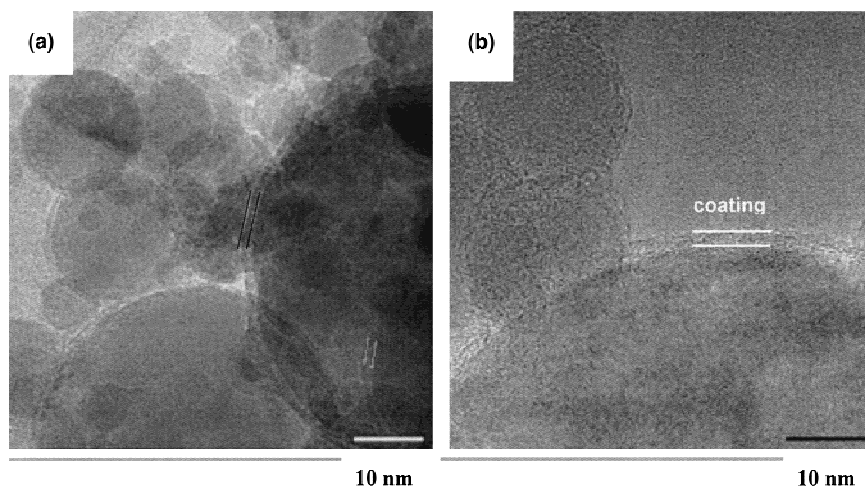

FIG. 3. (a) Bright-field TEM image of the coated alumina nanoparticles (scale bar = 20 nm). The coated layers are marked by the double lines. (b) HRTEM image showing the amorphous, pyrrole-coated nanoparticle surfaces (scale bar = 10 nm).
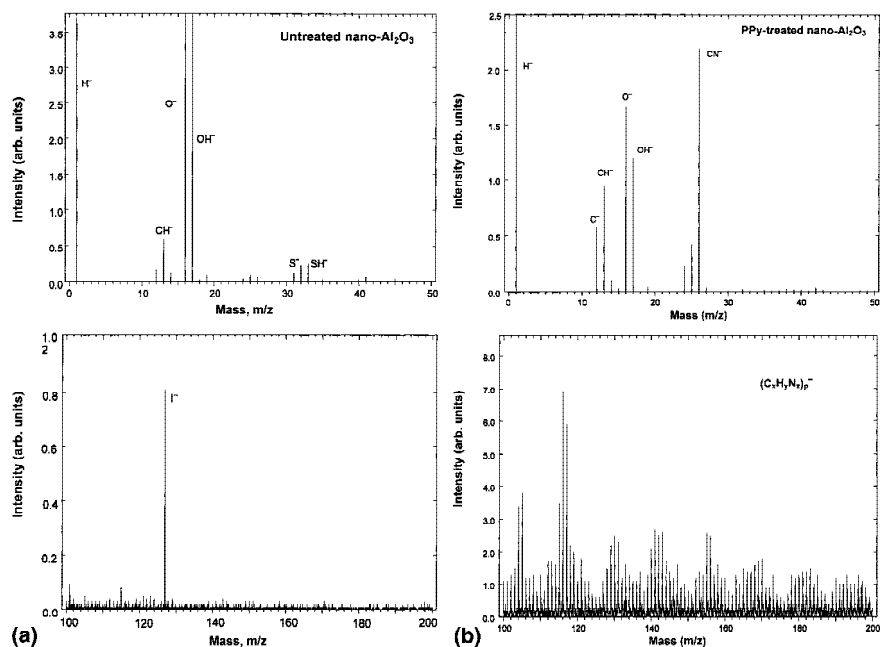
FIG. 4. TOFSIMS spectra if (a) untreated and (b) pyrrole-coated nanoparticles of alumina.

nitrogen-containing functionalities. The intense peak of Al$^+$ at +27 m/z (not shown in Fig. 4) is not the result of an incomplete coverage of the particles by the plasma polymer, but is caused by the intense sputtering of aluminum atoms from the particle surface during the initial phase of the plasma film deposition.[8] Consistent with this view is the absence of magnesium in the spectrum of the treated powder. The aluminum atoms or ions are incorporated in the first five nanometers of the plasma polymer film.

To further analyze the coated films, infrared (ir) experiment was performed on the coated nanoparticles. The ir spectrum is shown in Fig. 5(a). For comparison the ir spectrum of pyrrole monomer film was also obtained as shown in Fig. 5(b). In Figs. 5(a) and 5(b), both spectra exhibit strong peaks at about 3340 cm^{-1}, which correspond to the N–H stretching vibration of primary and secondary amines and imines. Also in Figs. 5(a) and 5(b) the absorption around 1640 cm^{-1} belongs to the amines in the pyrrole structure. In Fig. 5(a), there are two peaks at 2963.38 and 2934.44 cm^{-1}, but they are not present in Fig. 5(b). The peak at 2963.38 cm^{-1} is asymmetric CH$_3$ stretch and the peak at 2934.44 is asymmetric CH$_2$ vibration, respectively. In the structure of pyrrole monomer, all the carbon atoms are unsaturated without –CH$_3$ and –CH-function groups. However, after plasma coating, some –CH$_3$ function groups have formed due to plasma polymerization. This is evident on the absorption peaks at 2963.38 and 2934.44 cm^{-1} in Fig. 5(a). Furthermore, a peak at 722.455 cm^{-1} in Fig. 5(a) is related to the –(CH$_2$)$_n$-structure for n > 4, another strong evidence of polymerization of the pyrrole structure.
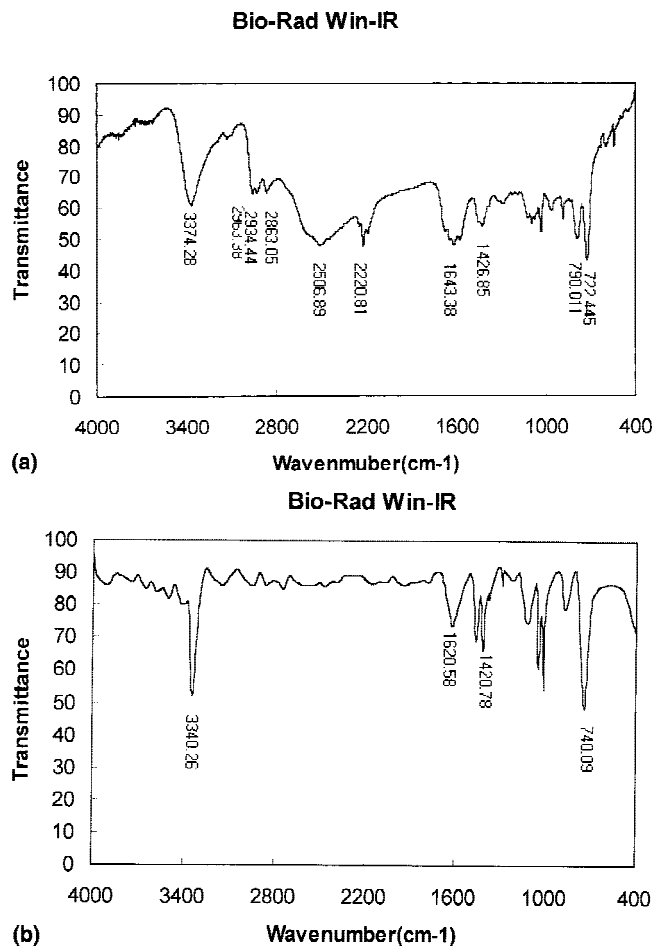
Bio-Rad Win-IR

(a)

Bio-Rad Win-IR

(b)

FIG. 5. (a) ir spectrum of plasma-coated pyrrole film and (b) ir spectrum of pyrrole monomer.

Figure 6 shows the SEM micrographs of consolidated alumina with and without polymer coating. Both samples were heat treated at 250 °C for 60 min. As can be seen in Fig. 6(a), the uncoated particles exhibit a highly porous structure as expected, since there is no sintering effect at such a low temperature. In contrast, under the same heat-treatment condition, the coated particles adhere to each other resulting in a dense matrix as shown in Fig. 6(b). The density of the coated sample is estimated to be at least 95%, which is comparable to that of a high-temperature sintered counterpart.

As we heat treated these samples at a much higher temperature, the microstructure showed rapid grain growth, however, in an inhomogeneous fashion. As exemplified in Fig. 7(a), a sample heat treated at 250 °C for 360 min showed a highly densified matrix. Figure 7(b) shows the surface of a sample that was heat treated at 800 °C for 360 min. As can be seen, the grain growth is evident but only in some local regions. Due to this localized grain growth, internal stress is not evenly distributed. At this temperature we assume that the polymer coating has been entirely decomposed and the effect of sintering sets in.

Although this research is mainly focused on the study of interface adhesion, we have carried out the heat treatment at much higher temperatures such as 1000 °C for

comparison purposes. At 1000 °C, the polymer film in the sample should completely decompose; however, the C–C bonds still remain between particles. These bonds can be responsible for considerable interface attraction among particles. The coated polymer film can also change the surface energy, which leads to a better dispersion of particles. Figure 8 shows the SEM images of the sample that was heat treated at 1000 °C for 12 h. As can be seen in Fig. 8, the polymer coating, although entirely burned out at this temperature, has resulted in significant microstructural difference. We have found that the sample with the polymer coating [Fig. 8(b)] is considerably denser than that of the noncoated one [Fig. 8(a)]. The grain size of the uncoated sample is also noticeably larger than its coated counterpart.

Figure 9(a) shows the microhardness values for the samples that were heat treated up to 800 °C for 60 min. The nanoparticles used in these samples before consolidation were coated with the thin films of pyrrole. The short heat-treatment time was to ensure that no sintering effect would result at elevated temperatures. As can be seen in Fig. 9, there is not significant change in microhardness from the samples heat treated in such a wide temperature range, suggesting a similar particle-to-particle bonding mechanism. However, above 350 °C, no adhesive polymer thin film should exist on nanoparticle
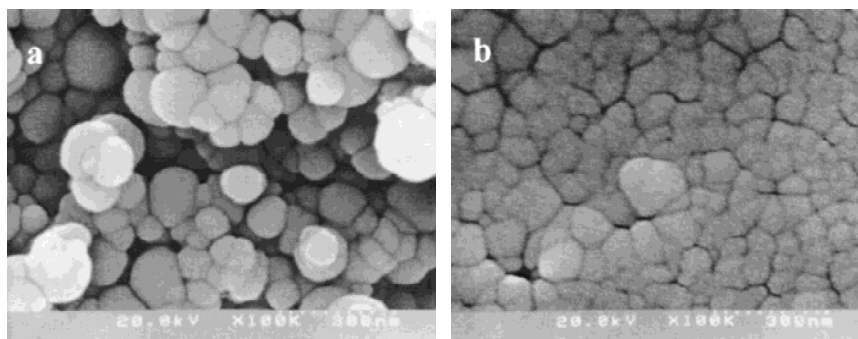

FIG. 6. SEM micrographs showing the consolidated alumina (a) with and (b) without pyrrole coating. Both samples were heat treated at 250 °C for 60 min.
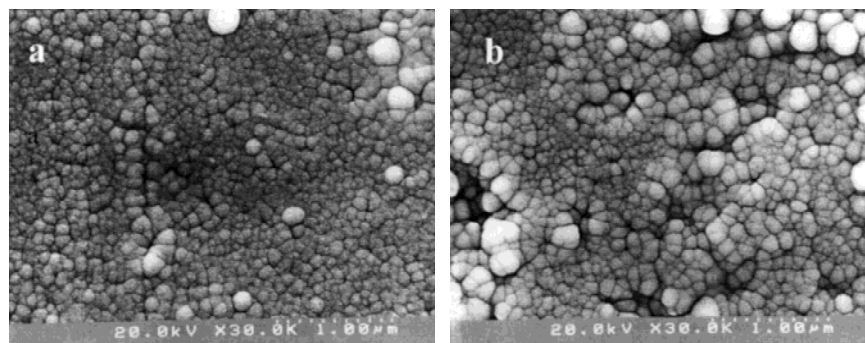

FIG. 7. SEM micrographs showing (a) the sample heat treated at 250 °C for 360 min and (b) the sample heat treated at 800 °C for 360 min. Both were pyrrole coated.
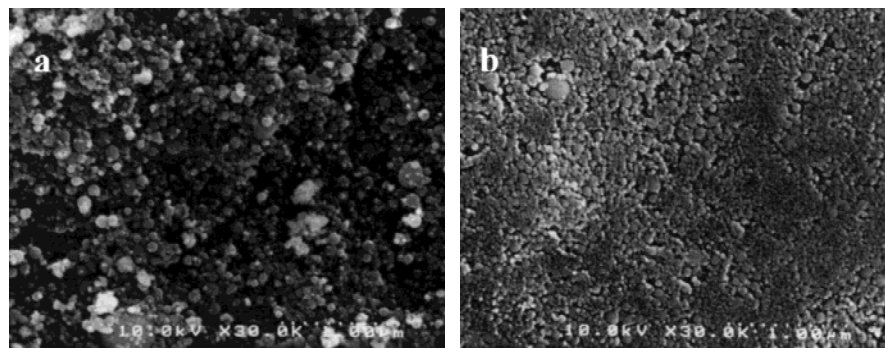
FIG. 8. SEM micrographs showing the samples heat treatment at 1000 °C for 12 h for (a) uncoated and (b) coated nanoparticles.

surfaces that may cause the gradual decrease in micro-hardness above this temperature. Figure 9(b) shows microhardness values versus heat-treatment time for consolidated alumina nanoparticles at heat-treatment temperatures indicated. As can be seen, the heat-treatment time does not seem to have a significant effect on microhardness. This may also be an indication that the adhesive film is responsible for bonding in this range of temperature and time. The exact consolidation procedure was also applied to uncoated nanoparticles of alumina. However, their micro-hardness values were found to be about 30 times less than those shown in Fig. 9.

To study the interface adhesive behavior we have carried our HRTEM experiments on the consolidated nanoparticles. Figure 10 shows the HRTEM images of the pyrrole-coated alumina nanoparticles. In these images, the crystal Al$_2$O$_3$ lattice is quite apparent with the amorphous polymer film at the particle interfaces. It is also apparent that there is a layer of NSA between the nanoparticles, which is extremely thin, on the order of a few nanometers. The thin films on the nanoparticles exhibited roughened surfaces as shown in Fig. 10 that is in contrast to the smooth surfaces shown in Fig. 3. Such a deformed surface appears to be a result of particle-particle debonding during the breaking of the clusters for TEM experiment. The rough surfaces also indicate the adhesive characteristics of the interfacial bonding between the nanoparticles. In Fig. 11, we can see that the alumina nanoparticle interfaces appear to be "glued" together with pyrrole elastically deformed. Both edges of the joint also appear to be curved, indicating a quite flexible pyrrole film at the interfaces.

For conventional processing of ceramics, we need to review the sintering mechanism that is responsible for the densification and consolidation of the bulk materials. At much higher temperatures, sintering takes place, which can be described by a two-sphere model.[1] Because of the difference in chemical potential of two spheres, the concentration of vacancies beneath a concave surface is higher than beneath a flat or convex surface.

The transport of vacancies from a concave surface can occur by the mechanisms of lattice and boundary diffusion, with a concomitant flow of atoms in the opposite direction. The effect is pore rounding and a decrease in the total surface free energy. In the intermediate and final stages, the densification behavior is very dependent on the association of pores with grain boundaries and the rate and mode of grain growth. Diffusion of atoms across the grain boundary, the disordered region between grains, causes the grain boundary to be displaced. Heating causes
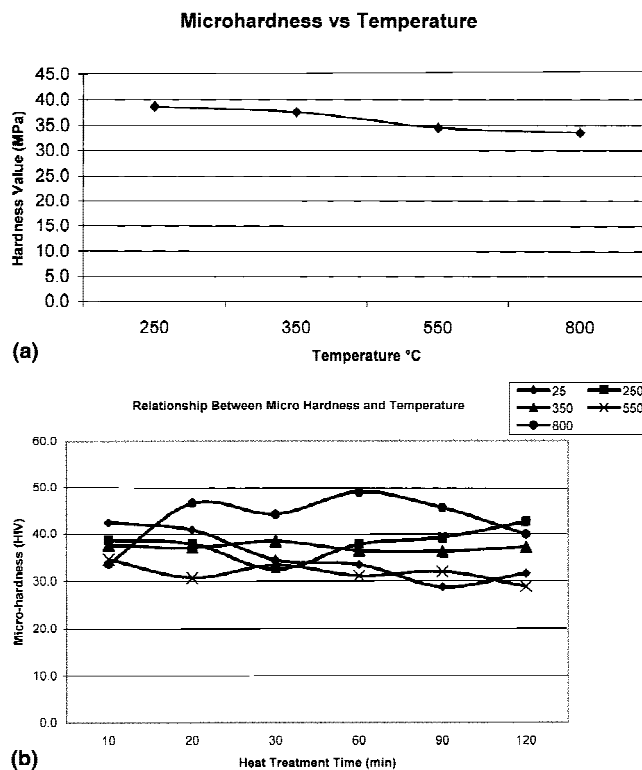

(a)

(b)

FIG. 9. (a) Microhardness vs temperature for the samples that were heat treated up to 800 °C for 60 min and (b) microhardness vs heat-treatment time at the heat-treatment temperatures indicated. Note that the alumina nanoparticles in the samples shown in this figure were coated with pyrrole thin films before consolidation.
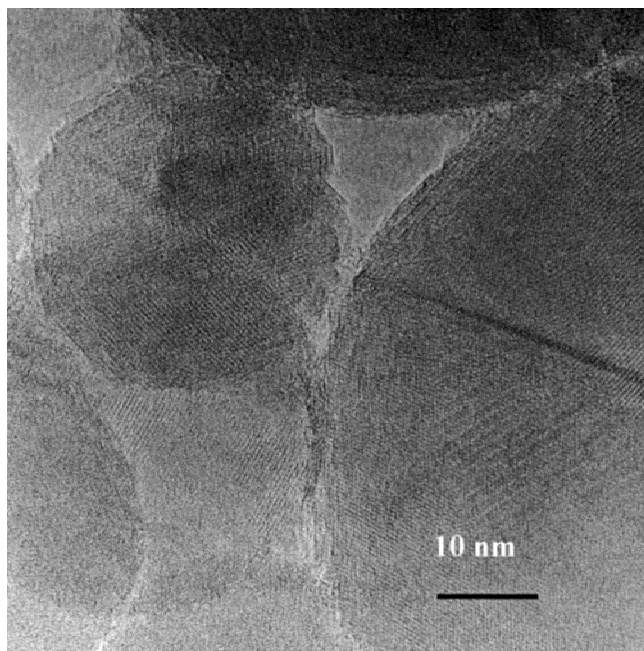
FIG. 10. Bright-field TEM image of the coated alumina nanoparticles that have been consolidated at 250 °C for 360 min (scale bar = 10 nm). The coated layer surfaces are roughened due to debonding indicating an adhesive behavior at the nanoscale.
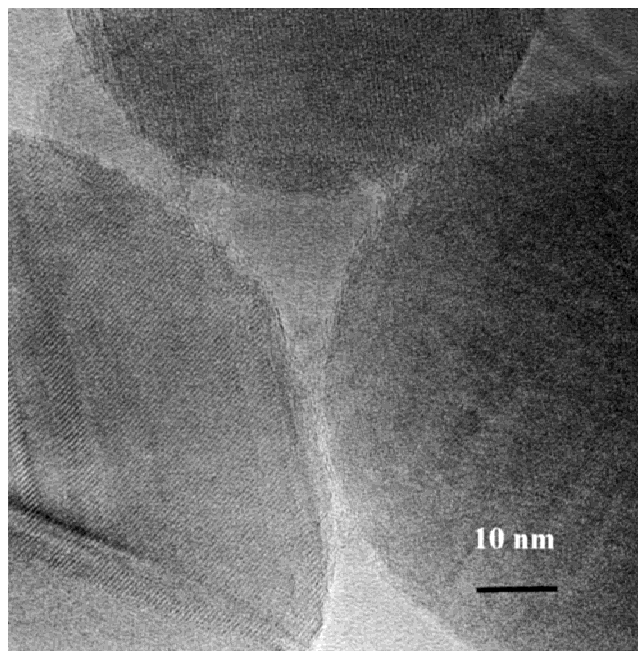

FIG. 11. TEM image of the same sample shown in Fig. 9 with the elastically deformed adhesive layer at the particle interfaces (scale bar = 10 nm).

some grains to grow at the expense of others that shrink, and the net effect is an increase in the mean grain size and a reduction in the total grain boundary area. However, the grain growth will diminish the characteristics of nanoparticles. The purpose of the NSA concept is to achieve the similar density and strength without high-temperature treatment.

A challenge in the area of nanomaterials is associated with the limited theoretical models that can explain the new nanostructures and their unique properties. Theory analysis is still not well established to explain the mechanical and chemical behaviors between that involving individual nanoparticles at the one extreme and that involving "bulk" materials at the other. Currently nearly all explanations in this aspect are based on large-scale interfaces rather than nanointerfaces. Yet, one may be able to extrapolate the current adhesion concepts into nano-domain where we have no direct information for the NSA-induced bonding.

Two major mechanisms of adhesion that we may consider for coated nanoparticles are mechanical interlocking and adsorption theory.[9–14]

The theory of mechanical interlocking essentially proposes that mechanical keying, or interlocking, of the adhesive into the irregularities of the substrate surface is the major source of intrinsic adhesion. However, the attainment of good adhesion between smooth surfaces exposes this theory as not being of wide applicability. And, considering the role of mechanical interlocking, it is

firstly debatable whether mechanical interlocking really does occur and secondly, even if it does, to assess its contribution to the strength and stability of the interface is difficult. However, on the basis of this theory, mechanical interlocking occurs on a large-scale surface roughness of the order of several hundred microns. Hardly can it be used to explain the interfacial adhesion when the particle size decreases sharply to the order of nanometer.

The molecular forces in the surface layers of the adhesive and substrate greatly influence the attainment of intimate molecular contact across the interface, called the adsorption. The attainment of interfacial contact is invariably a necessary first stage in the formation of strong and stable adhesive joints. The next stage is the generation of intrinsic adhesion forces across the interface, and the nature and magnitude of such forces are extremely important. They must be sufficiently strong and stable to ensure that the interface does not act as the "weak link" in the joint, either when the joint is initially made or throughout its subsequent service life.[15]

Other mechanisms include the diffusion and the electronic theories.[15,16–18] In the diffusion theory, the intrinsic adhesion of polymers is established through mutual diffusion of polymer molecules across the interface. This requires that the macromolecules, or chain segments of the polymers (adhesive and substrate) possess sufficient mobility and are mutually soluble. In a nanostructured medium, the coated particles are compacted by a three-dimensional network with multiple interfaces

around an individual nanoparticle. The diffusional process is therefore fundamentally different from the planar interface adhesion.

The electronic theory treats the adhesive/substrate systems as a capacitor that is charged due to the contact of the two different materials.[15] Separation on the parts of the capacitor, as during the interface rupture, leads to a separation of charge and to a potential difference, which increases until a discharge occurs. Adhesion is presumed to be due to the existence of these attractive forces across the electrical double layer. The adsorption theory states that the materials will adhere because of the interatomic and intermolecular forces, which are established between the atoms and molecules in the interfaces of the adhesive and substrate. Again, these theories apply to macroscopic interfaces and cannot easily be used to model the nanoparticle interfaces, although these mechanisms are assumed to exist.

Therefore, to study the fundamental mechanism of adhesion between nanoparticles, new theoretical modeling work is required for a varied nanosurface structure. As such, a mathematical model has to be developed to study particle-particle adhesion instead of a flat surface macroscopic adhesion. Our current work is focused on the modeling work based on the results of the tensile test.

The cylindrical sample is made of polymer-coated nanoparticles pressed at room temperature and slightly heated below the burnout temperature of the polymer (approximately 350 °C). The sample is subjected to a tensile stress as shown in Fig. 12. It is assumed that the tensile stress σ_z and strain ϵ_z are the same everywhere in the adhesive layer on the top and bottom of the particles. We further assume that the nanoparticles are ordered adhesively in a simple packing shown in Fig. 13(a). Certainly, this is a quite simplified situation, and we assume the lateral deformation is negligible. We also assume the tensile stress is uniform and the shear stress, τ_{rz}, is zero. The radial, σ_r, and the circumferential, σ_θ, stresses are assumed to be the same. It has been
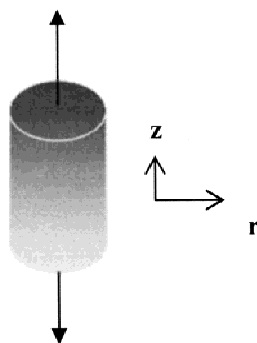

FIG. 12. Tensile test for the modeling of adhesive mechanism of nanoparticles.
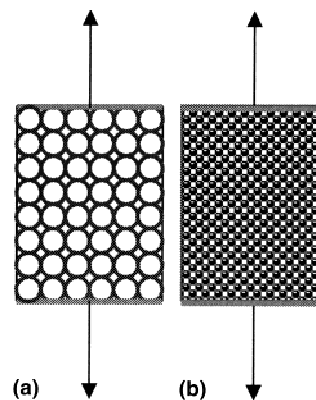

FIG. 13. (a) Particle configuration with a simple packing and (b) particle configuration with a more complicated triangle packing.

shown[19] that the radial and circumferential strains in the adhesive layers are equal to the Poisson's ratio strain in the nanoparticles. Thus

$$1/E_a(\sigma_\theta - v_a[\sigma_z + \sigma_\theta]) = 1(v_n/E_n)\, \sigma_z \quad,$$

hence

$$\sigma_\theta = \sigma_r = [v_a - E_a v_s/E_s][\sigma_z/(1 - v_a)] \quad,$$

where v_a is the Poisson's ratio of the adhesive, and the subscripts "a" and "s" refer to adhesive and nanoparticles, respectively. Hence, in the central region of an axially loaded nanojoint the adhesive layers are subjected to traxial tensile stresses.

It has been reported that, for a macroscopic flat butt joint, the fracture stress increased as the thickness of the adhesive layer decreased. The explanations were based either upon the presence of higher internal stress or upon the larger flaws in the relatively thicker adhesive layers. We can use the above model to calculate the apparent Young's modulus (defined as the ratio of the applied tensile stress over the strain across the adhesive layer, i.e., σ_0/σ_z), and fit the experimental data of the tensile experiments for different processing conditions including coating thickness, particle size, and consolidation parameters (pressure and temperature). By varying these parameters, the fitting of the experimental data can provide valuable information on the microscopic adhesion mechanism. Better fitting will be obtained as we assume more complicated configurations of nanoparticles in the bulk, one of which is shown in Fig. 13(b). We can assume more realistic configurations by choosing the best fitted curves of experimental data. However, the results of modeling work will not be included in this paper.

Although from the HRTEM imagines in Figs. 10 and 11, it is obvious that the nanoparticles are "glued" together, the underlying adhesion mechanism is yet to be identified. Because the mechanical interlocking requires

micron-scale roughness, it cannot be applied to nanoscale surfaces. Therefore, the absorption theory of adhesion may be a more appropriate approach to our problem in this study. On the basis of this model, if sufficiently intimate molecular contact is achieved at an interface, the material will adhere due to the interatomic and intermolecular forces that are established between the atoms and molecules in the surfaces of the adhesive and substrate. Commonly these are Van der Waals forces and referred to as secondary bonds. In addition, chemical bonds may sometimes be formed across the interface. This is termed "chemisorption" and involves ionic, covalent, or metallic interfacial bonds being established; these bonds are referred to as primary bonds.[15] It is believed that the interfacial bonding between nanoparticles is through an adsorption mechanism. Due to the nature of secondary bonding, the individual adhesive force may not be as strong as mechanical interlocking, however, the overall bonding strength may be improved if the total interfacial surface area is significantly increased. For nanoparticles this is possible considering their large surface areas.

Nanoparticles are known to have extremely high surface areas.[20–27] As a result of the high surface area, the surface energy can reach the order of 100 kJ/mol for a variety of materials. McHale *et al.* have reported experimental data on the surface energies of alumina nanoparticles.[27] They have found that γ–Al$_2$O$_3$ can maintain surface areas of 150 m^{2}g^{-1} at 1073 K. However, α–Al$_2$O$_3$ coarsens to values <50 m^{2}g^{-1} at the same temperature. Based on these findings, they concluded that γ–Al$_2$O$_3$ should be energetically stable polymorph as the specific surface area exceeds approximately 125 m^{2}g^{-1}. During film deposition, the polymer is introduced as a vapor and the collision frequency increases with the gas pressure. Due to the high surface energy of the nanoparticles, condensation of the polymer vapor on the nanoparticles naturally lowers the surface energy by forming an extremely thin film. On a large two-dimensional flat substrate, however, the deposition of the film may cluster severely and form small islands initially, due to its surface tension. A smooth film will require continued deposition at an appreciable thickness. In our deposition process, both energy terms (surface energy of the nanoparticle and the surface tension of the polymer) were balanced by controlling the plasma coating parameters including electron density, temperature, and energy density. The gas pressure must be moderate for a low collision rate on the nanoparticle surfaces. In addition, polymerization should take place relatively fast after the condensation on the particle surfaces. These will ensure a uniform coating on the order of 2 nm for all particles sizes. Such an ultrathin and uniform film provides the foundation for the nanoscaled adhesive between the nanoparticles.

IV. SUMMARY

In summary, we have deposited an ultrathin film of pyrrole on the surface of alumina nanoparticles by means of a plasma polymerization treatment. The polymer layer is not only uniform on all particle sizes, but also extremely thin with a thickness of 2 nm. Such ultrathin film deposition characteristics are essential in establishing multilayer nanostructures, particularly for adhesive bonding at nanoparticle interfaces. With such a thin polymer film on nanoparticles we have been able to observe, by means of HRTEM, a unique adhesive behavior at the nanoparticle interfaces. Based on this adhesive film we have consolidated the nanoparticles at temperatures much lower than sintering temperature. Although the operating adhesion mechanism requires further studies we believe, based on the experimental data from this study, that intrinsic adhesion forces are responsible for the observed interfacial bonding. Our future work will focus on the interface study in terms of structure, adhesion behavior, and related mechanical properties. Improved adhesive coatings will also be selected for coating of the nanoparticles.

REFERENCES

1. J.S. Reed, *Principles of Ceramics Processing,* 2nd ed. (John Wiley & Sons, Inc., New York, 1988).
2. J.E. Buek and J.H. Rosolowski, in *Treatise on Solid State Chemistry,* edited by N.B. Hannay (Plenum, New York, 1976), Vol. 4.
3. J.P. Singh, D. Shi, and D.W. Capone, Appl. Phys. Lett. **53,** 239 (1987).
4. D. Shi, D.W. Capone II, G.T. Goudey, J.P. Singh, N.J. Zaluzec, and K.C. Goretta, Mater. Lett. **6,** 217 (1988).
5. J.P. Singh, H.J. Leu, R.B. Poeppel, E. van Voorhees, G.T. Goudey, K. Winsley, and D. Shi, J. Appl. Phys. **66,** 3154 (1989).
6. K.C. Goretta, O.D. Lacy, U. Balachandran, D. Shi, and J.L. Routbort, J. Mater. Sci. Lett. **9,** 380 (1990).
7. S. Eufinger, W.J. van Ooij, and T.H. Ridgway, J. Appl. Pol. Sci. **61,** 1503 (1996).
8. W.J. van Ooij, S. Eufinger, and T.H. Ridgway, Plasma and Polymers, **1,** 231 (1996).
9. R.W. Siegel, Nanostructured Materials, **3,** 1 (1993).
10. J.R. Huntsberger, in *Treatise on Adhesion and Adhesives,* edited by R.L. Patrick (Mercel Dekker, New York, 1967), Vol. 1.
11. J.T. Dickson, L.C. Hensen, S. Lee, L. Scudiero, and S.C. Langford, J. of Adhesion Sci. Technol., **8,** 1285 (1994).
12. R.G. Horn, D.T. Smith, and A. Grabbe, Nature **366,** 442 (1993).
13. R.G. Horn and D.T. Smith, Science **256,** 362 (1992).
14. J.N. Israelachvili, J. Coll. Interface Sci. **44,** 259 (1973).
15. A.J. Kinloch, *Adhesion and Adhesives* (Chapman and Hall, London, United Kingdom, 1987).

16. F.M. Fowkes, Ind. Eng. Chem. **56,** 40 (1964).
17. A.J. Kinloch, W.A. Dukes, and R.A. Gledhill, in *Adhesion Science and Technology,* edited by L.H. Lee (Plenum Press, New York).
18. E.P. Plueddemann, *Silane Coupling Agents* (Plenum Press, New York, 1982).
19. A.J. Kinloch, *Adhesion and Adhesives* (Chapman and Hall, London, United Kingdom, 1987).
20. G.C. Hadjipanayis and R.W. Siegel, *Nanophase materials, Synthesis-properties-applications* (Kluwer Press, Dordrecht, Germany, 1994).
21. G.M. Whitesides, J.P. Mathias, and C.T. Seto, Science **254,** 1312 (1991).
22. C.D. Stucky and J.E. MacDougall, Science **247,** 669 (1990).
23. H. Gleiter, Nanostructured Materials, **6,** 3 (1995).
24. A.T. Wolde, *Nanotechnology,* ED. (STT Netherlands Study Center for Technology Trends, The Hague, The Netherlands, 1998).
25. N. Inagaki, S. Tasaka, and K. Ishii, J. App. Poly. Sci., **48,** 1433 (1993).
26. C. Bayer, M. Karches, A. Mattews, and P.R. von Rohr, Chem. Eng. Technol. **21,** 427 (1998).
27. J.M. McHale, A. Auroux, A.J. Perrotta, and A. Navrotsky, Science **277,** 188 (1997).